Systemic Delivery of Liposomal Short-Chain Ceramide Limits Solid Tumor Growth in Murine Models of Breast Adenocarcinoma

Thomas C. Stover, Arati Sharma, Gavin P. Robertson, and Mark Kester

Abstract *In vitro* tumor cell culture models have illuminated the potential therapeutic utility of elevating the intracellular concentration of the antimitogenic and proapoptotic sphingolipid, ceramide. However, although cell-permeable, short-chain ceramide is an effective apoptotic agent *in vitro*, its use as an *in vivo*, systemically delivered therapeutic is limited by its inherent lipid hydrophobicity and physicochemical properties. Here, we report that the systemic i.v. delivery of C_6-ceramide (C_6) in a pegylated liposomal formulation significantly limited the growth of solid tumors in a syngeneic BALB/c mouse tumor model of breast adenocarcinoma. Over a 3-week treatment period, a well-tolerated dose of 36 mg/kg liposomal-C_6 elicited a >6-fold reduction in tumor size compared with empty ghost liposomes. Histologic analyses of solid tumors from liposomal-C_6-treated mice showed a marked increase in the presence of apoptotic cells, with a coincident decrease in cellular proliferation and in the development of a microvessel network. Liposomal-C_6 accumulated within caveolae and mitochondria, suggesting putative mechanisms by which ceramide induces selective cancer cell cytotoxicity. A pharmacokinetic analysis of systemic liposomal-C_6 delivery showed that the pegylated liposomal formulation follows first-order kinetics in the blood and achieves a steady-state concentration in tumor tissue. Confirming the therapeutic utility of i.v. liposomal-C_6 administration, we also shown diminution of solid tumor growth in a human xenograft model of breast cancer. Together, these results indicate that bioactive ceramide analogues can be incorporated into pegylated liposomal vehicles for improved solubility, drug delivery, and antineoplastic efficacy.

Sphingolipids not only serve a structural role in membranes but also are substrates for the generation of bioactive second messengers that influence mitogenesis and apoptosis. Metabolism of sphingomyelin, the major sphingolipid in membranes, forms ceramide, a potent lipid-derived second messenger that modulates the induction of cell differentiation, cell cycle arrest, and/or apoptosis (1–4). In addition, chemotherapeutic agents (5–7) and ionizing radiation (8, 9) are two of the multiple cellular stressors (10–16) that lead to the accumulation of ceramide within membranes. We and others have shown that ceramide-mediated signaling cascades induce apoptosis in part via the inhibition of Akt prosurvival pathways, mitochondrial dysfunction, and the stimulation of caspase activity, which ultimately leads to DNA fragmentation and cell death (17–21).

Although short-chain, cell-permeable ceramides, such as C_6-ceramide (C_6), have been shown to be antiproliferative and proapoptotic in numerous cancer cell types *in vitro* (22, 23), there are obstacles to the delivery of ceramide for systemic applications, such as cancer chemotherapy. Despite being more efficacious than physiologic long-chain ceramides (C_{18}-C_{24}-ceramide), the effectiveness of cell-permeable ceramide analogues remains limited due to their inherent hydrophobicity and potential precipitation as fine lipid micelle suspensions when given in aqueous solutions (24). Thus, to realize the therapeutic benefits of ceramide bioactivity, there is a need for improved drug delivery systems to assist with solubility, cell permeability, protection from enzymatic degradation, and systemic administration.

We and the Mayer laboratory have shown that ceramide-incorporated liposomes are more cytotoxic than nonliposomal ceramide delivered via organic solvents (21, 25, 26). Our studies showed that C_6-incorporated pegylated liposomes significantly inhibited proliferation and induced apoptosis in human MDA-MB-231 breast adenocarcinoma cells (21). In addition, stable ceramide-containing liposomes exhibited an increase in life span of >20% in the J774 ascites tumor model compared with control liposomes following i.v. bolus and i.p. administration (26). The present study extends these findings to a solid tumor model of mammary adenocarcinoma. Our studies not only show the efficacy of inhibiting solid tumor growth following i.v. administration of liposomal-C_6 but also documents the underlying biophysical mechanisms of delivery of ceramide leading to tumor cell cytotoxicity.

Authors' Affiliation: Department of Pharmacology, Pennsylvania State College of Medicine, Hershey, Pennsylvania
Received 8/30/04; revised 1/28/05; accepted 2/9/05.
Grant support: NIH grant HL66371.
The costs of publication of this article were defrayed in part by the payment of page charges. This article must therefore be hereby marked *advertisement* in accordance with 18 U.S.C. Section 1734 solely to indicate this fact.
Note: M. Kester participates in a related but separate project sponsored in part by REVA Medical, Inc., San Diego, CA.
Requests for reprints: Mark Kester, Department of Pharmacology, Pennsylvania State College of Medicine, P.O. Box 850, Hershey, PA 17033. Phone: 717-531-8964; Fax: 717-531-5013; E-mail: mxk38@psu.edu.

Materials and Methods

Materials and cell culture. 1,2-Dioleoyl-*sn*-glycero-3-phosphocholine, 1,2-dioleoyl-*sn*-glycero-3-phosphoethanolamine, *N*-hexanoyl-D-erythro-sphingosine (C_6), 1,2-distearoyl-*sn*-glycero-3-phosphoethanolamine-*N*-[methoxy polyethylene glycol-2000], *N*-octanoyl-sphingosine-1-[succinyl(methoxy polyethylene glycol-750)] (PEG(750)-C_8), *N*-[6-[(7-nitro-2-1,3-benzoxadiazol-4-yl)amino]hexanoyl]-D-erythro-sphingosine (NBD-C_6), and *N*,*N*-dimethyl-D-erythro-sphingosine (DMSph) were purchased from Avanti Polar Lipids (Alabaster, AL). *N*-hexanoyl-D-erythro-sphingosine [hexanoyl 6-^{3}H] ([^{3}H]C_6) was obtained from ARC (St. Louis, MO). Primary antibodies to caveolin-1 and CD31 were purchased from Santa Cruz Biotechnology (Santa Cruz, CA) and BD PharMingen (San Jose, CA), respectively. Horseradish peroxidase–conjugated goat anti-rabbit IgG and rhodamine red-X–conjugated goat anti-rat IgG secondary antibodies were obtained from Santa Cruz Biotechnology and Jackson ImmunoResearch Laboratories, Inc. (West Grove, PA), respectively. For pharmacokinetic studies, Solvable aqueous-based tissue solubilizer was purchased from Perkin-Elmer (Wellesley, MA). Murine 410.4 mammary adenocarcinoma cells were a kind gift from Dr. Amy Fulton (University of Maryland, Baltimore, MD) and grown at 37°C in RPMI 1640 supplemented with 10% fetal bovine serum. This cell line is a highly aggressive murine metastatic tumor cell line cultured from a BALB/c mouse lineage (27). Normal murine HC11 mammary epithelial cells, also from a BALB/c mouse lineage, were a kind gift from Dr. Bernd Groner (University of Frankfurt am Main, Frankfurt am Main, Germany) and grown at 37°C in RPMI 1640 supplemented with 10% fetal bovine serum, 10 ng/mL epidermal growth factor, and 5 μg/mL insulin. Human MDA-MB-231 breast adenocarcinoma cells were obtained from American Type Culture Collection (Manassas, VA) and grown at 37°C in RPMI 1640 supplemented with 10% fetal bovine serum. MDA-MB-231 is a highly aggressive human metastatic, estrogen receptor–negative, breast cancer cell line.

Liposome formulation. Lipids were solubilized in chloroform, combined in a specific molar ratio [1,2-dioleoyl-*sn*-glycero-3-phosphocholine/1,2-dioleoyl-*sn*-glycero-3-phosphoethanolamine/1,2-distearoyl-*sn*-glycero-3-phosphoethanolamine-*N*-[methoxy PEG(2000)]/PEG(750)-C_8/C_6 (3.75:1.75:0.75:0.75:3.0 molar ratio)], dried under a stream of nitrogen above the lipid transition temperatures for each lipid, and hydrated with sterile isotonic 0.9% NaCl solution. The resulting solution underwent sonication for 2 minutes followed by extrusion through 100 nm polycarbonate membranes using the Avanti Mini Extruder (Avanti Polar Lipids). Incorporation efficiency was determined as described previously (21) by incorporating trace amounts of [^{3}H]C_6 into the formulation, extracting constituent lipids in chloroform/methanol (2:1), and comparing radioactivity levels of equal aliquots before and after extrusion using a scintillation counter. In preliminary studies, there was no significant loss of C_6 during the formulation of liposomal vesicles. Moreover, liposomal-C_6 vesicles were formulated with an average size of 84 nm as measured by dynamic light scattering. The composition of formulated liposomes was validated by extracting constituent lipids in chloroform/methanol (2:1) followed by resolution on preheated silica gel 60 TLC plates using a chloroform/methanol/double-distilled water (60:25:4) solvent system. Lipids were visualized in an iodine chamber.

Cell cytotoxicity studies. To characterize the antiproliferative effects of liposomal-C_6 on normal and cancerous murine mammary epithelial cells, murine HC11 mammary epithelial cells and 410.4 mammary adenocarcinoma cells were plated out at 6×10^3 per well in 96-well tissue culture plates. The following day, the cells were treated in their normal culture medium with liposomal-C_6, ghost liposomes, nonliposomal "free" C_6, and DMSO vehicle at the indicated doses for 48 hours. As a positive control for cell cytotoxicity, HC11 cells were also treated with DMSph. Following the 48-hour treatment, cell cytotoxicity was assessed using the Cell Titer 96 aqueous nonradioactive cell proliferation assay (Promega, Madison, WI) following manufacturer's instructions. The assay employs a tetrazolium compound that is bioreduced by viable cells into a soluble formazan product, which can be measured by absorbance at 490 nm. The quantity of formazan product as measured by its absorbance is directly proportional to the number of viable cells in culture.

Cell apoptosis analysis. As described previously (21), ceramide-induced apoptosis was assessed and quantified by flow cytometric analysis of Annexin V–stained cells using the Vybrant Apoptosis Assay Kit 3 (Molecular Probes, Eugene, OR). Briefly, 410.4 mammary epithelial cells were plated at 4×10^5 per plate in 60 mm tissue culture plates. Following a 24-hour treatment with 25 μmol/L liposomal-C_6, adherent cells were harvested by trypsinization and all cells (floating and adherent) were washed once with cold PBS and pelleted at $300 \times g$. Pelleted cells were then stained with FITC-labeled Annexin V and propidium iodide according to the manufacturer's instructions. Labeled cells were immediately analyzed using flow cytometry. Viable cells were double negative, early apoptotic cells were positive for Annexin V staining and negative for propidium iodide staining, and late apoptotic cells were double positive. Cells positive for propidium iodide but negative for Annexin V were considered to be necrotic or debris and were excluded from apoptotic cell analysis.

In addition to Annexin V staining, an *In situ* Cell Death Detection kit (Roche Diagnostics Corp., Indianapolis, IN) was used, following the manufacturer's instructions, to confirm the induction of apoptosis. Briefly, 410.4 mammary epithelial cells were plated at 4×10^5 per plate in 60 mm tissue culture plates and treated with 25 μmol/L liposomal-C_6, nonliposomal-C_6, and vehicle controls for 24 hours. Following treatment, adherent cells were harvested by trypsinization and all cells (floating and adherent) were washed once with PBS, fixed with 2% paraformaldehyde, permeabilized with 0.1% Triton X-100, and treated with terminal deoxynucleotidyl transferase in the presence of fluorescein-labeled nucleotide polymers. Terminal deoxynucleotidyl transferase–mediated dUTP nick end labeling (TUNEL)-positive cells were immediately analyzed using flow cytometry to quantify the induction of apoptosis. A one-color analysis, excluding small cellular debris, was done.

Confocal studies. To verify cell accumulation of C_6 into 410.4 murine mammary adenocarcinoma cells, we formulated a liposomal-C_6 vesicle with 10 molar percent NBD-C_6 as a marker for C_6. Cells were plated at 2.0×10^4 per well in eight-well chamber slides and allowed to grow overnight. Liposomal-NBD-C_6 was treated at 25 μmol/L for a 2-hour treatment period. Cellular nuclei were counterstained with 4′,6-diamidino-2-phenylindole and MitoTracker Deep Red 633 (Molecular Probes) was used as a marker for mitochondria following manufacturer's instructions. C_6 delivery and accumulation was evaluated by confocal microscopy at ×63 magnification (Leica Microsystems, Heidelberg, Germany).

Sucrose gradient and Western blot. To evaluate whether ceramide preferentially accumulates into caveolin-1-enriched lipid rafts (known as caveolae), we did a sucrose gradient of cellular lysate as described previously (28). This velocity gradient centrifugation procedure permits the isolation of caveolin-1-enriched lipid raft microdomains within a cellular lysate. The liposomal-C_6 formulation was incorporated with trace amounts of [^{3}H]C_6 to monitor C_6 levels. Briefly, 410.4 cells were plated at 1.5×10^6 per plate into 100 mm tissue culture plates and grown to ~90% confluency. Cells were treated with 25 μmol/L tritiated liposomal-C_6 for the indicated time points. Cells were lysed in 2 mL of 500 mmol/L $NaCO_3$ buffer containing 1 mmol/L phenylmethylsulfonyl fluoride and 1 mmol/L $NaVO_3$ and subsequently homogenized using a Dounce glass homogenizer. Cell lysates were mixed 1:1 (v/v) with 90% sucrose in 25 mmol/L MES (pH 6.5) and 0.15 mol/L NaCl (final 45% sucrose) and loaded into Beckman (Fullerton, CA) ultracentrifuge tube. The 45% sucrose solution was then overlayed with 4 mL of 35% sucrose/$NaCO_3$ solution and then 4 mL of 5% sucrose/$NaCO_3$ solution to form a 5%-35%-45% sucrose gradient. Samples were centrifuged at 35,000 rpm for 18 hours using a SW-40ti rotor. The 12 mL gradient was then aliquoted into 1 mL fractions. Equal aliquots of 800 μL were removed

from each fraction and counted using a scintillation counter to assess ceramide levels. In addition, 50 μL of each fraction were loaded onto a Nupage 4% to 12% precasted SDS-PAGE gradient gel and probed for caveolin-1, which was visualized using enhanced chemiluminescence.

In vivo *syngeneic mammary adenocarcinoma tumor model.* To assess the *in vivo* efficacy of systemic liposomal-C_6 delivery in an immunocompetent, syngeneic solid tumor model, 5×10^6 410.4 cells were injected s.c. into the right hind flank of female BALB/c mice, which were purchased from Charles River Laboratories (Wilmington, MA). Four days later, when tumor size averaged 3 × 3 mm, tumor-bearing mice were randomized into seven groups with five mice per group. The mice received i.v. tail vein injections of either liposomal-C_6 (12, 24, or 36 mg/kg C_6) or empty ghost liposomes (equivalent total lipid mass as ceramide treatment group); the seventh group remained untreated. Mice were treated every 2 days, and immediately before treatment, mice were weighed and tumors were measured. Tumor size was measured with calipers, and tumor volume was calculated using the following formula: $V = (L \times W^2) / 2$, where V is tumor volume, L is length, and W is width. The study was halted when control tumors reached ~14 mm in diameter ~21 days following tumor cell injection.

In vivo *human breast cancer xenograft tumor model.* Further animal experimentation was done in athymic female nude mice, which were purchased from Harlan Sprague-Dawley (Indianapolis, IN). Tumor kinetics was measured by s.c. injection of 1×10^7 MDA-MB-231 cells in 0.2 mL DMEM containing 10% fetal bovine serum above the left and right rib cages of 4- to 6-week-old nude mice. Based on the data obtained from the syngeneic tumor model, xenograft tumor-bearing mice were initially treated every 2 days with 36 mg/kg liposomal-C_6 or empty ghost liposomes (equivalent total lipid mass as ceramide treatment group). We also chose to use an escalating dose regimen (36-72 mg/kg) to further evaluate efficacy versus possible systemic toxicology. Three dimensional tumor size was measured on alternate days with calipers, and tumor volume was calculated using the following formula: $V = (L \times W \times H)$, where V is tumor volume, L is length, W is width, and H is height. All of the animal studies were approved by the Institutional Animal Care and Use Committee at the Pennsylvania State College of Medicine (Hershey, PA).

Syngeneic tumor histology. A thorough histologic analysis was done to validate tumor growth inhibition. Tumors were removed from tumor-bearing mice following 1-week treatment with 40 mg/kg liposomal-C_6 and frozen in an ethanol/dry ice bath, and cryosections (4 microns) were generated for histologic analysis. To assess the degree of C_6-induced cellular apoptosis, tumor sections were stained using the *In situ* Cell Death Fluorescein Detection kit (Roche Diagnostics) following the manufacturer's instructions. Briefly, cryosections were fixed in 4% paraformaldehyde and permeabilized in 0.1% Triton X-100. Fixed and permeabilized cells were then incubated with TUNEL reaction mixture for 1 hour at 37°C in a humidified chamber. Positive control slides were treated with 300 units/mL DNase I for 10 minutes at 37°C to induce DNA strand breaks before the TUNEL labeling procedure.

Immunohistochemical procedures were used to evaluate proliferation and endothelial microvessel development in tumor tissue. To analyze proliferation, frozen sections were fixed in 4% paraformaldehyde, permeabilized with 0.2% Triton X-100 for 30 minutes at room temperature, and blocked with 5% normal donkey serum for 2 hours at room temperature. A goat anti-Ki-67 primary antibody (1:50) in 1% bovine serum albumin was applied to the tissue and incubated overnight at 4°C. A donkey anti-goat secondary antibody conjugated to rhodamine red-X was then applied (1:800) for 2 hours at room temperature in the dark. For microvessel endothelial cell staining, frozen sections were blocked with 10% normal goat serum and 1% bovine serum albumin for 2 hours at room temperature. A CD31 primary antibody (1:50) in 1% bovine serum albumin was applied to the tissue and incubated overnight at 4°C. A goat anti-rat secondary antibody conjugated to rhodamine red-X (1:800) was then applied for 2 hours at room temperature in the dark. All tissue sections were then mounted in 4′,6-diamidino-2-phenylindole-containing Vectashield mounting medium and visualized on a Leica confocal microscope using ×63 magnification. All histologic staining was quantified using the Leica confocal microscope software image analysis tools, which quantifies the number of pixels that represents positive staining, denoted "pixelation".

In vivo *pharmacokinetic analysis.* To show that pegylated liposomes can be effectively employed to systemically deliver short-chain ceramide to solid tumor tissue, we evaluated the pharmacokinetic distribution of i.v. given liposomal-C_6 in 410.4 syngeneic tumor-bearing mice. Using [^{3}H]C_6 as a marker for C_6 delivery, we injected tumor-bearing mice with 10 and 40 mg/kg liposomal-C_6 and removed blood (via cardiac puncture), tumor, spleen, kidney, liver, and heart tissue at chosen time points. Excised tissues were weighed, solubilized with Solvable, and counted using a scintillation counter. Using the specific activity of [^{3}H]C_6 (20 Ci/mmol), we calculated the mass of [^{3}H]C_6 within each tissue from the measured dpm counts. The mass of total C_6 per milligram of tissue (or milliliter of blood) was based on the fixed ratio (0.0026%) of [^{3}H]C_6 to total C_6 in the liposome formulation and the apparent ceramide concentration was calculated for each tissue removed. Control tissue from mice that were not injected with radiolabeled C_6 was removed to subtract background dpm counts from treated tissues, and a pharmacokinetic profile was generated. WinNonLin software (Pharsight Corp., Mountain View, CA) was employed to analyze the pharmacokinetic data using a two-compartment model of drug distribution and elimination. A two-compartment model has wider application than a one-compartment model, because the body is divided into a central compartment with rapid mixing and a peripheral compartment with slower distribution.

Statistical analysis. Differences among two treatment groups were statistically analyzed using a two-tailed Student's t test for statistical analyses. Differences among three or more groups were analyzed using a one-way ANOVA test. A statistically significant difference was reported with Ps indicated where applicable. Data are reported as the mean ± SE from at least three separate experiments. Specifically, for both syngeneic and nude experiments, a quadratic random coefficient model was fit to tumor growth curves for each treatment group (29). The quadratic random coefficient model accounts for the repeated measurements over time. From the quadratic random coefficient model, 2 df contrasts (for the linear and quadratic coefficients) were used to compare any given two tumor growth curves. A Bonferroni correction was made to the Ps to account for the multiple comparisons testing of the tumor growth curves within the syngeneic experiment. All analyses were done using the SAS statistical software, particularly the ROBUSTREG and MIXED procedures (SAS Institute, Inc., Cary, NC).

Results

Liposomal-C_6-ceramide induces adenocarcinoma cellular cytotoxicity and apoptosis. The liposomal-C_6 formulation was first tested for its *in vitro* cytotoxic effects in murine 410.4 mammary adenocarcinoma cells. The delivery of C_6 in our pegylated liposomal formulation reduced the IC_{50} >2-fold from 12 to 5 μmol/L for nonliposomal-C_6 and liposomal-C_6, respectively. Our pegylated formulation displayed an improved dose-response inhibition of growth in 410.4 cells compared with nonliposomal "free" administration of C_6 in DMSO vehicle (Fig. 1A), thus indicating improved potency and efficacy. A pegylated "ghost" formulation without C_6 did not significantly affect 410.4 cell cytotoxicity, confirming previous studies noting that pegylated components (PEG(750)-C_8 and 1,2-distearoyl-*sn*-glycero-3-phosphoethanolamine-*N*-[methoxy PEG(2000)]) are not cytotoxic (21). Similar cytotoxicity profiles were observed in another highly aggressive and metastatic murine adenocarcinoma cell line, T41 (ref. 30; data not shown),

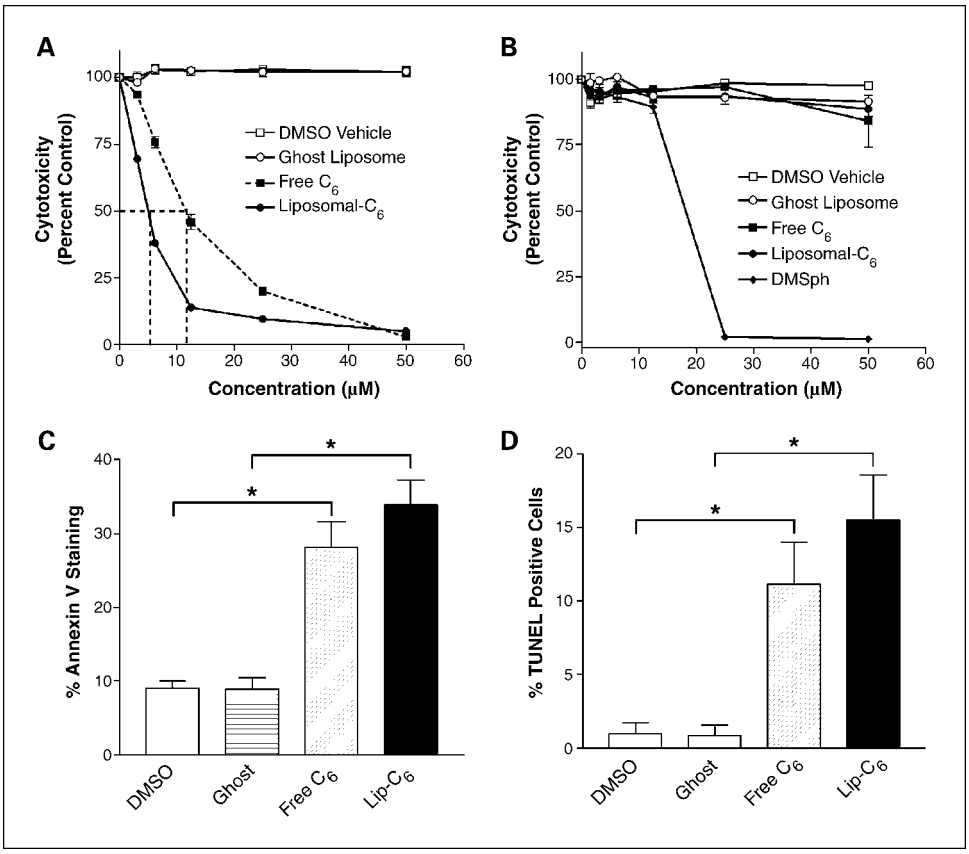

Fig. 1. Liposomal-C_6 delivery resulted in an enhanced, dose-dependent, cellular toxicity in cancerous mammary epithelial cells but not in normal mammary epithelial cells. *A*, in 410.4 mammary epithelial adenocarcinoma cells, liposomal-C_6 lowered the observed IC_{50} of C_6, compared with free administration of C_6 in DMSO vehicle, as assessed by MTS assay. *B*, neither liposomal-C_6 nor free C_6 was cytotoxic in normal HC11 mammary epithelial cells. DMSph, a positive control for lipid-induced cytotoxicity, was cytotoxic for HC11 cells. *C*, Annexin V staining showed that 25 μmol/L liposomal-C_6 induced a greater degree of cellular apoptosis in 410.4 cells compared with nonliposomal "free" C_6. *D*, 25 μmol/L liposomal-C_6 induced a significant increase in TUNEL-positive apoptotic 410.4 cells. As a positive control for the TUNEL assay, DNase treatment (300 units/mL) of fixed untreated 410.4 cells resulted in 75.5 ± 14.3% TUNEL-positive staining. *, $P < 0.05$, when comparing pegylated liposomal-C_6 and free C_6 cytotoxicity to pegylated ghost and DMSO vehicle, respectively.

alluding to the potential applicability of liposomal-C_6 delivery as an experimental therapeutic. This *in vitro* study indicates that a pegylated liposomal formulation designed for systemic drug delivery is an effective vehicle for C_6-mediated induction of murine 410.4 mammary adenocarcinoma cell cytotoxicity.

In contrast to the murine 410.4 mammary adenocarcinoma cells, normal murine HC11 mammary epithelial cells did not show increased cytotoxicity to either liposomal-C_6 or "free" C_6 in DMSO vehicle (Fig. 1B). However, as a positive control, DMSph was toxic to the HC11 cells. DMSph is a known proapoptotic agent that shares the characteristic sphingoid backbone of all sphingolipids, including ceramide. DMSph inhibits sphingosine kinase activity, ultimately resulting in accumulation of ceramide as well as reduction in the prosurvival metabolite sphingosine-1-phosphate (31). This study shows the potential utility of C_6 as a chemotherapeutic with limited side effects, because the liposomal-C_6 formulation preferentially targets tumorigenic versus normal mammary epithelial tissue, a finding consistent with other *in vitro* studies using ceramide analogues (32, 33).

We next investigated if C_6-dependent growth inhibition correlated with enhanced apoptosis in 410.4 cells. To confirm that C_6 delivery leads to cell apoptosis, we did Annexin V staining of treated cycling 410.4 cells. Annexin V stains phosphatidylserine on the outer leaflet of apoptotic cells, a hallmark of apoptosis. Following a 48-hour treatment at 25 μmol/L, liposomal-C_6 induced a significantly greater amount of Annexin V staining compared with nonliposomal-C_6, whereas the ghost formulation had no effect (Fig. 1C). A TUNEL assay was used to confirm the Annexin V results. In a similar fashion, liposomal-C_6 induced a significant increase in TUNEL-positive 410.4 cells when compared with ghost formulations (Fig. 1D). Together, these cytotoxicity and apoptosis studies indicate that liposomal delivery of C_6 limits clonal expansion by promoting apoptosis in the 410.4 mammary adenocarcinoma cell line.

Liposomal-C_6-ceramide treatment allows preferential accumulation of C_6-ceramide in caveolae. We have shown previously that liposomal-C_6 partitions out of the liposomal bilayer into the plasma membrane bilayer without associated liposome/cell membrane fusion (21). We now extend these studies to assess if liposomal-C_6 accumulates within membrane rafts, sites of ceramide-regulated signaling cascades. Caveolin-1-enriched lipid rafts, or caveolae, are known to serve as signaling docking platforms for a multitude of signaling cascades (34, 35). We used trace amounts of [^{3}H]C_6 within the liposomal formulation to assess time-dependent cellular accumulation of 25 μmol/L C_6 in caveolin-1-enriched lipid rafts. Within 15 minutes, ceramide was observed to preferentially accumulate within fractions 4 to 5 of a sucrose gradient in which caveolin-1 was found to be localized (Fig. 2A). It was evident that as time progressed, a percentage of the delivered C_6 migrated to non-caveolin-1-enriched fractions. Consistent with previous studies (21), total accumulation of ceramide within cell lysates (fractions 1-12) was linear over a 6-hour time period. We confirmed these data with NBD-C_6, demonstrating that that both radiolabeled and fluorolabeled C_6 accumulate within caveolae. Specifically, following a 2-hour treatment, 69.1% of total cellular NBD-C_6 (compared with 63.5% of total cellular

[^{3}H]C_6) were observed to accumulate within caveolin-1-enriched fractions (4-5) of the sucrose gradient. Thus, the delivery of liposomal-C_6 allows for the early preferential accumulation of ceramide into caveolae, which have been implicated as potential initiation sites for intracellular signaling cascades, including those that ultimately lead to cellular apoptosis (34, 35).

Liposomal-C_6-ceramide treatment delivers C_6-ceramide to mitochondria. Studies have shown that ceramide acts on the mitochondria to initiate antiproliferative and proapoptotic effects (36). Thus, we hypothesized that exogenous C_6 treatment would result in an accumulation of ceramide in the mitochondria of 410.4 adenocarcinoma cells. Using MitoTracker Deep Red as a marker for mitochondria, we showed that 25 μmol/L liposomal-NBD-C_6 colocalized with this mitochondrial marker (Fig. 2B), signifying the accumulation of exogenous ceramide. This study indicates that liposomal-C_6 localizes within the mitochondria, possibly contributing to mitochondrial dysfunction and resultant cell death.

Liposomal-C_6-ceramide treatment displays dose-dependent antitumor activity in a syngeneic tumor model. To study the *in vivo* anticancer activity of systemically delivered liposomal-C_6 on solid tumor tissue, we inoculated 410.4 cells in the right hind flank of female BALB/c mice to induce solid tumors. Preliminary toxicology studies showed that female BALB/c mice tolerated a single i.v. liposomal-C_6 dose of up to 100 mg/kg with no evident side effects (data not shown). However, i.v. treatment with 10 mg/kg nonliposomal "free" C_6 in an 80% ethanol solution was lethal in 50% of the mice (LD_{50}, 10 mg/kg), whereas 80% ethanol alone displayed no lethality. The acute, dose-limiting toxicity observed with free C_6 may be attributed to the extreme hydrophobicity of the molecule and its propensity to precipitate immediately in

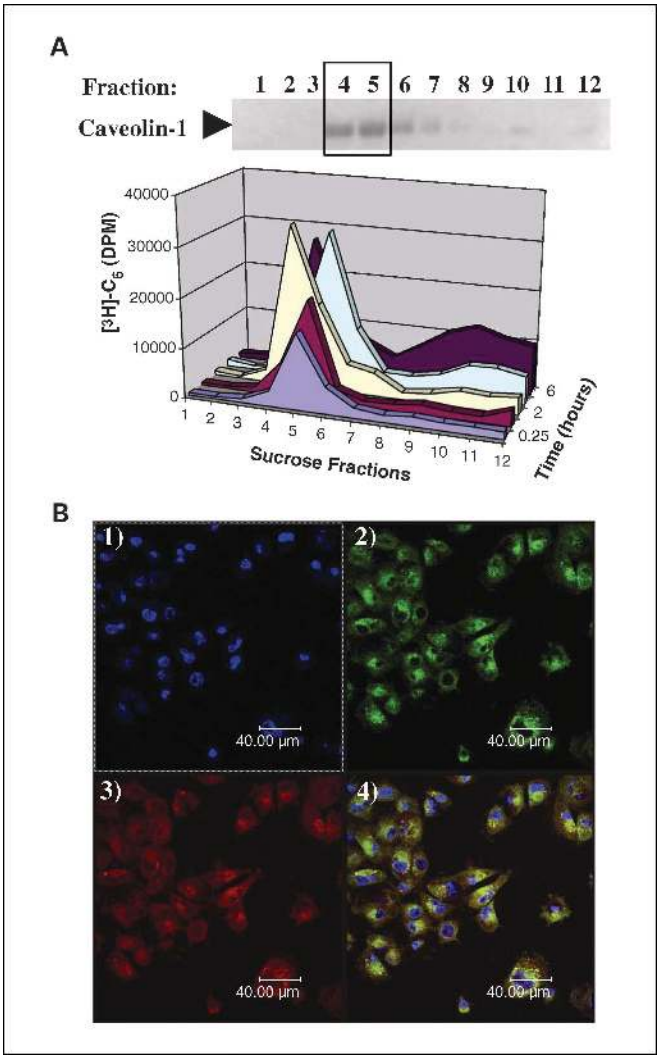

Fig. 2. Liposomal-C_6 delivery resulted in the preferential accumulation of C_6 in caveolae lipid rafts and in mitochondria of 410.4 mammary adenocarcinoma cells. *A*, time-dependent accumulation of 25 μmol/L C_6, represented by an increase in dpm counts of [^{3}H]C_6, was shown to preferentially accumulate within caveolin-1-enriched lipid rafts. C_6 accumulated in caveolin-1-enriched fractions 4 to 5 of a sucrose gradient of cellular lysate, a marker for caveolae lipid rafts. *B*, confocal microscopic images of 25 μmol/L liposomal-NBD-C_6 delivery to 410.4 cells showed that NBD-C_6 (*green*) colocalized with cellular mitochondria (*red*); cellular nuclei are stained with 4′,6-diamidino-2-phenylindole (*blue*). Magnification, ×63.

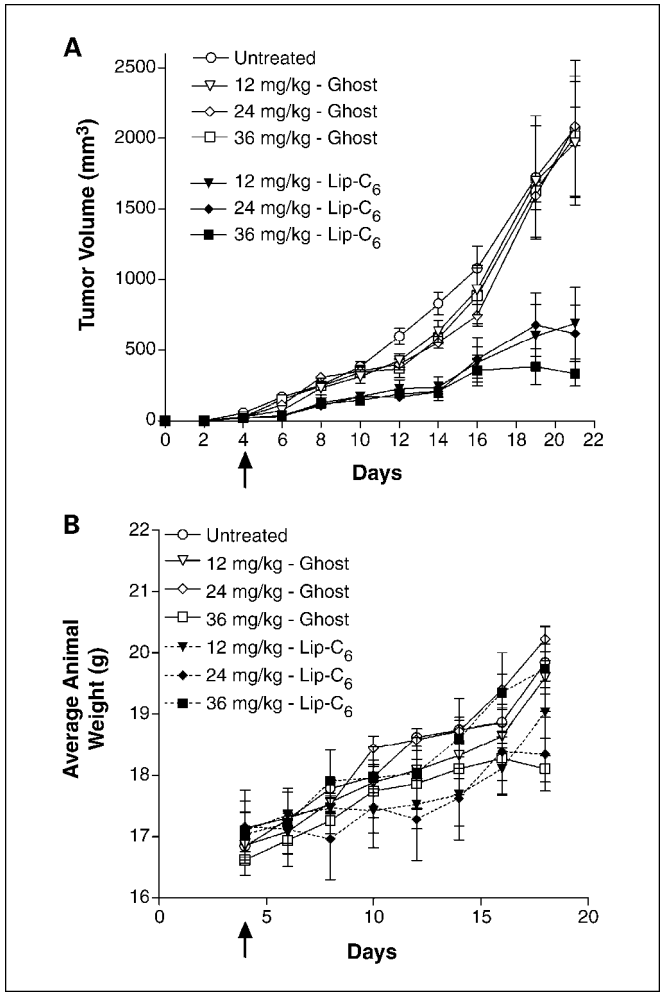

Fig. 3. Liposomal-C_6 delivery displayed dose-dependent antitumor activity in a syngeneic mouse solid tumor model of mammary adenocarcinoma. *A*, systemic delivery of liposomal-C_6 (*Lip-C_6*) through tail vein injection on alternate days significantly inhibited tumor growth in a dose-dependent manner compared with ghost liposome and untreated controls. The 36 mg/kg dose of liposomal-C_6 was statistically different ($P < 0.01$; $n = 5$ animals per group) than the equivalent ghost-treated group and the untreated group. *B*, average animal weights of liposomal-C_6 and ghost treatment groups or the untreated group did not significantly differ from one another, indicating that the liposomal-C_6 administration was not overtly toxic to the tumor-bearing mice.

aqueous solutions and possibly induce an occlusion. Thus, liposomal delivery of C_6 significantly reduces the LD_{50} when given i.v. in female BALB/c mice. It seems that in addition to serving as a suitable drug delivery vehicle our liposomal formulation has the further benefit of delivering ceramide in a much less toxic form.

Tumor-bearing mice were treated on an alternate day schedule with liposomal-C_6 or ghost liposomes via tail vein injections. Liposomal-C_6 treatments showed a significant dose-response inhibition of tumor growth compared with ghost and untreated controls (Fig. 3A). The greatest degree of tumor growth suppression was observed with the 36 mg/kg liposomal-C_6 formulation. All doses of the ghost formulation had no appreciable effects on tumor volume. The most significant tumor growth suppression was evident near the cessation of treatment, suggesting that liposomal-C_6 maintained its

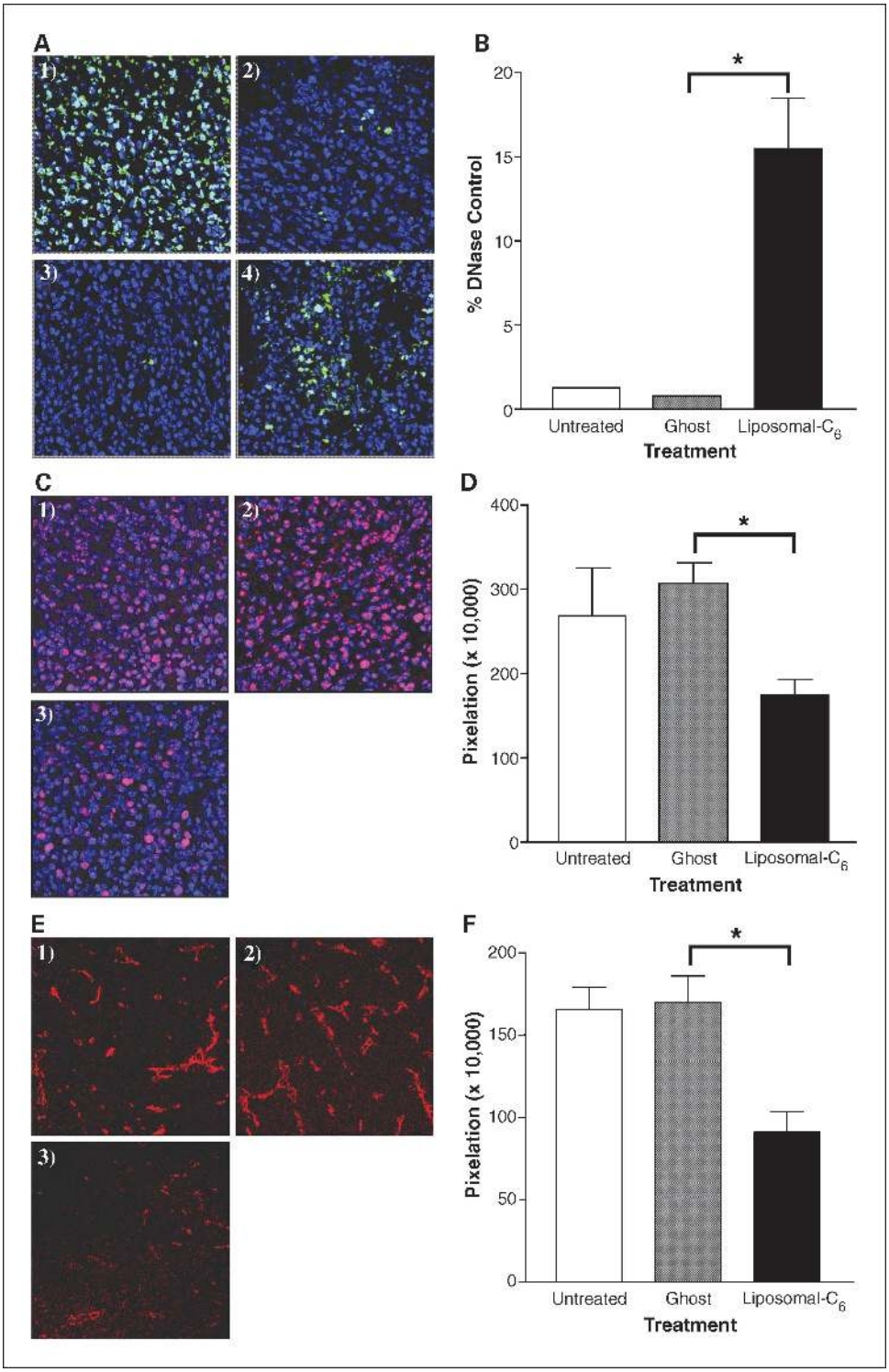

Fig. 4. Liposomal-C_6 induced cellular apoptosis, limited cellular proliferation, and limited microvessel growth within solid tumor tissue. *A*, tumor sections were stained with an *in situ* death fluorescein detection kit to assess the degree of cellular apoptosis via TUNEL-FITC staining (*green*); 4′,6-diamidino-2-phenylindole-stained nuclei (*blue*). Liposomal-C_6-treated tumors (*A-4*) showed more positive TUNEL staining than ghost (*A-3*) and untreated (*A-2*) control tumors. DNase I – treated tumor sections (*A-1*) were included as a positive control. *B*, quantification of TUNEL-FITC staining as a percentage of DNase I – positive control indicated that liposomal-C_6 induced significantly more apoptosis (~20-fold) within solid tumor sections than was seen with ghost-treated or nontreated control mice. *C*, tissue sections were stained for Ki-67 (*red*), a marker for cellular proliferation, and for nuclei (4′,6-diamidino-2-phenylindole stain; *blue*) resulting in significantly less staining for liposomal-C_6-treated tumors (*C-3*) compared with ghost-treated (*C-2*) and nontreated (*C-1*) controls. *D*, quantification of Ki-67 staining indicated that liposomal-C_6 significantly limited tumor cell proliferation by nearly 40% within solid tumor sections when compared with ghost-treated or nontreated control mice. *E*, tumor sections were stained with a primary antibody recognizing CD31, a specific marker for endothelial cells. Positively stained microvessels (*red*) indicate that liposomal-C_6 (*E-3*) limited microvessel growth in solid tumor tissue compared with ghost-treated (*E-2*) and untreated (*E-1*) controls. *F*, quantification of CD31 staining indicated that liposomal-C_6 significantly limited the endothelial microvessel development within tumor tissue by ~50% when compared with ghost-treated or nontreated control mice. $n = 4$ tumors per group. *, $P < 0.01$, when comparing pegylated liposomal-C_6 accumulation to pegylated ghost liposome. Magnification, ×63.

anticancer effects throughout the treatment period. At the cessation of tumor treatment on day 21, the mean tumor volume of the 36 mg/kg ghost-treated mice was ~6-fold higher than that of the 36 mg/kg liposomal-C_6-treated mice in the 410.4 solid tumor model ($P < 0.01$). Moreover, as the treatment period progressed, the average mouse weight for liposomal-C_6-treated mice did not vary significantly from ghost-treated or untreated mice (Fig. 3B), thus signifying that the liposomal-C_6 treatment regimen did not display systemic toxicity to the tumor-bearing mice.

***Liposomal-C_6-ceramide treatment induces tumor apoptosis and reduces cellular proliferation* in vivo.** To validate that liposomal-C_6 induced apoptosis, resulting in diminished tumor growth, we did an immunofluorescent analysis of frozen tumor sections. Tumor sections were stained using an *in situ* TUNEL assay, which stains the nicked ends of DNA, a marker for cellular apoptosis. Tumor tissue from mice treated with liposomal-C_6 (Fig. 4A-4) had significantly more TUNEL staining than those of ghost-treated (Fig. 4A-3) or untreated mice (Fig. 4A-2). As a positive control, DNase I–treated tissue sections displayed marked TUNEL staining (Fig. 4A-1). Liposomal-C_6 treatment resulted in nearly a 20-fold increase in cellular apoptosis when compared with ghost treatment (Fig. 4B). Consistent with these apoptosis data, we also show that liposomal-C_6 (Fig. 4C-3) is more efficacious than ghost (Fig. 4C-2) or untreated mice (Fig. 4C-1) as measured by Ki-67 staining for proliferation. In fact, liposomal-C_6 treatment resulted in an ~40% decrease in cellular proliferation (Fig. 4D). These studies show that the liposomal delivery of C_6 to solid tumor tissue induces significant apoptotic death, leading to limited tumor growth.

***Liposomal-C_6-ceramide treatment reduces tumor microvessel formation* in vivo.** Further histologic analysis of frozen tumor tissue showed that liposomal-C_6 treatment (Fig. 4E-3) resulted in significantly less staining for CD31, a marker for endothelial cells, when compared with ghost-treated (Fig. 4E-2) or untreated mice (Fig. 4E-1). Tumors treated with liposomal-C_6 displayed nearly a 50% decrease in CD31 staining when compared with ghost-treated and untreated mice (Fig. 4F). We propose that in addition to inducing cellular apoptosis liposomal-C_6 inhibits the development of a microvessel network within solid tumor tissue, thus restricting the angiogenic-dependent growth of the solid tumor mass.

Liposomal-C_6-ceramide treatment displays favorable pharmacokinetic variables, consistent with its antitumor efficacy. To quantify the concentration of C_6 in various tissues following systemic i.v. administration in the 410.4 syngeneic tumor model, we again incorporated trace amounts of [^{3}H]C_6 into the liposomal-C_6 formulation to serve as a marker for total C_6. Blood concentrations of liposomal-C_6 seemed to follow linear first-order kinetics following i.v. administration (Fig. 5A).

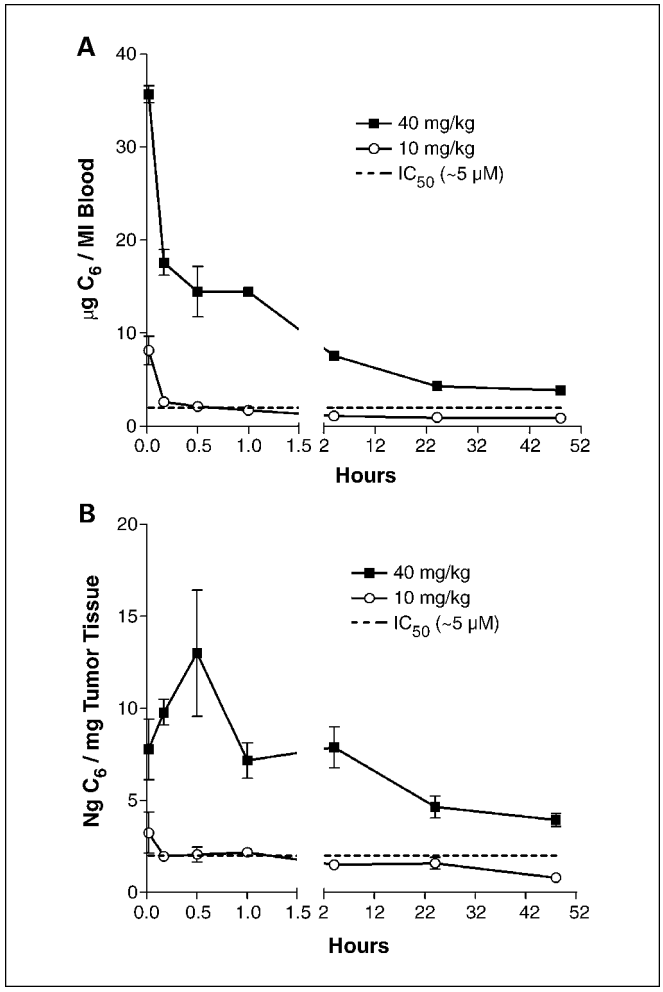

Fig. 5. Blood and tumor concentrations of bioactive C_6 in tumor-bearing mice were maintained over a 48-hour period. *A*, 10 and 40 mg/kg doses of liposomal-C_6 followed first-order kinetics, with a blood concentration exceeding the *in vitro* IC_{50} sustained at 48 hours. *B*, at these doses, a steady-state concentration of C_6 in the tumor tissue was achieved at ~60 minutes. The 40 mg/kg dose maintained a concentration above the desired IC_{50} up to 48 hours. $n = 4$ tumors per group.

Table 1. *In vivo* pharmacokinetic tissue distribution for liposomal-C_6 in a BALB/c mouse 410.4 mammary adenocarcinoma solid tumor model

	ng C_6/mg tissue					
Time (h)	Blood	Tumor	Spleen	Kidney	Liver	Heart
0.01667	35.67 ± 1.30	5.94 ± 0.46	31.93 ± 2.20	73.86 ± 3.98	116.27 ± 20.84	88.05 ± 3.63
0.1667	17.60 ± 1.94	9.21 ± 0.52	31.70 ± 2.68	167.11 ± 24.99	50.81 ± 17.86	67.24 ± 9.32
0.5	14.46 ± 3.87	8.12 ± 1.51	23.15 ± 6.17	104.91 ± 29.99	25.56 ± 6.90	34.49 ± 12.77
1	12.77 ± 2.12	7.27 ± 0.36	14.99 ± 3.38	48.08 ± 2.29	12.99 ± 2.36	21.79 ± 1.66
4	7.53 ± 0.12	8.42 ± 0.40	8.10 ± 1.11	17.66 ± 1.26	6.93 ± 0.48	10.83 ± 0.64
24	4.30 ± 0.33	5.65 ± 0.14	5.17 ± 0.54	7.95 ± 1.61	5.95 ± 0.54	6.70 ± 1.30

Using a 40 mg/kg dose, blood concentrations of liposomal-C_6 were maintained well above the *in vitro* IC_{50} concentration (~5 μmol/L) throughout a 48-hour period. This concentration of liposomal-C_6 in the blood allows for the accumulation and maintenance of bioactive concentrations in the solid tumor tissue (Fig. 5B). Table 1 presents the tissue distribution profile in the blood, tumor, liver, kidney, spleen, and heart over a 48-hour period following i.v. administration of 40 mg/kg liposomal-C_6. Although a relative steady-state bioactive concentration of liposomal-C_6 is achieved within the tumor tissue, it is apparent that ceramide is rapidly cleared from the most highly perfused, first-pass organs that we analyzed. Using a two-compartmental model of distribution, Table 2 presents the associated pharmacokinetic variables of systemic liposomal-C_6 delivery in the blood. It is noteworthy that based on this kinetic modeling analysis that the apparent $t_{1/2}$ is ~11 hours for the liposomal-C_6 formulation, further supporting the utility of these drug delivery vehicles. It is therefore concluded that liposomal-C_6 delivery not only improves the solubility of C_6 and fosters accumulation within tumor tissue but also allows for the sustained/controlled release of the drug over time, reducing the acute toxicity of C_6 and limiting tumor growth *in vivo*.

Liposomal-C_6-ceramide treatment displays antitumor activity in a human xenograft tumor model. To confirm and extend the above results from the syngeneic solid tumor model, we next evaluated the efficacy of a 36 mg/kg dose of liposomal-C_6 in a human xenograft nude mouse tumor model of breast adenocarcinoma. We chose human MDA-MB-231 breast adenocarcinoma cells, as we have shown previously that this highly metastatic, estrogen receptor–negative cell line responds to liposomal-C_6 with marked apoptosis *in vitro* (21). *In vitro* ceramide-induced apoptosis was validated previously using multiple methodologies, including Annexin V staining, TUNEL analysis, caspase stimulation, and propidium iodide labeling (21). We now report that the i.v. administration of liposomal-C_6, at an initial 36 mg/kg dose, statistically limits xenograft tumor growth upward of 5 weeks (Fig. 6). Despite an early reduction in tumor growth at this dose, it seemed that tumors developed some degree of resistance to treatment at approximately day 30. Thus, we escalated the dose to 72 mg/kg on day 32 for the duration of the study to potentially improve efficacy without inducing toxicity. This higher dose seemed to result in a short-term effect on efficacy without inducing apparent systemic toxicology. Although we show for the first time that systemic liposomal-C_6 delivery can limit tumor growth in both syngeneic and human xenograft models, it may require a combinatorial therapeutic approach to fully limit or regress solid tumors. It can be envisioned that additional chemotherapeutic agents with distinct mechanisms of action can be coencapsulated within ceramide-incorporated liposomes.

Table 2. Two-compartmental pharmacokinetic modeling for systemic liposomal-C_6 delivery in a BALB/c mouse

Liposomal-C_6 plasma variables	
$Time_{max}$ (min)	0
$Concentration_{max}$ (ng/mg)	38.5826
$Time_{final}$ (min)	1,440
$Concentration_{final}$ (ng/mg)	4.3
Area under the curve (min * ng/mg)	9,698.469
$t_{1/2}$ (min)	677.8695
Observed clearance (mg/min * ng/mg)	0.0029

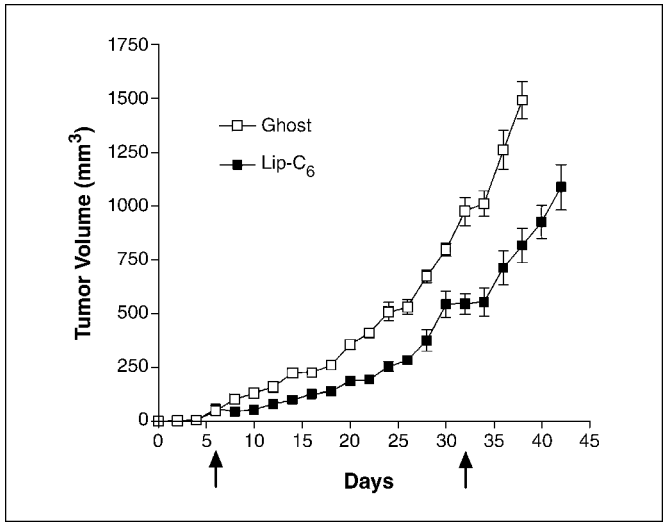

Fig. 6. Liposomal-C_6 delivery displayed antitumor activity in a human xenograft solid tumor model of breast adenocarcinoma. Systemic delivery of 36 mg/kg (days 6-30) and 72 mg/kg (days 32-40) liposomal-C_6 through tail vein injection on alternate days significantly inhibited tumor growth compared with ghost liposomes ($P < 0.0001$, $n = 5$ animals per group, each N represents the mean of two tumors).

Discussion

Many studies, including our own, have shown that ceramide can effectively induce apoptosis in tumor cells *in vitro* (23, 37). However, the potential chemotherapeutic utility of ceramide is limited by its inherent hydrophobicity. Using syngeneic and human xenograft models of breast adenocarcinoma, we now show that C_6-incorporated stable liposomes are an optimal "solution" for selective, bioefficacious, systemic delivery of ceramide. We designed the formulation to carry a large ratio of C_6, a bilayer-destabilizing lipid, to maximize the drug payload without sacrificing vesicular stability. The inclusion of PEG(750)-C_8 stabilized the formulation, allowing for the incorporation of up to 30 molar percent C_6. PEG(750)-C_8 is composed of a 750 molecular weight PEG head group conjugated to the free hydroxyl of C_8-cermamide. Without the PEG(750)-C_8, stable vesicles containing 30 molar percent C_6 could not be prepared or extruded. Additionally, the inclusion of PEG(750)-C_8 has been observed to facilitate time-release properties of liposomal bilayers with the added benefit of enhanced bioavailability due to the PEG chains (38).

Using this liposomal formulation, we investigated the membranous localization of liposomal-C_6 in 410.4 murine adenocarcinoma cells. We observed two distinct pools of exogenously delivered ceramide that are consistent with the ability of ceramide to induce apoptosis in breast cancer cells. First, endogenous ceramide preferentially accumulates within caveolin-1-enriched lipid rafts, structured microdomains that regulate the dynamic interaction between signaling molecules (34, 39, 40). In addition, the spontaneous ability of endogenous ceramide to partition into and expand lipid raft microdomains

may also regulate signaling cascades within these lipid rafts (37, 40, 41). Ceramide-mediated inhibition of the prosurvival kinase Akt seems to occur within these caveolin-1-enriched domains.[1] Ceramide has been shown to target and activate protein kinase Cζ (17), which phosphorylates Akt at Thr^{34} (42), contributing to the observed apoptotic cell death (43). A second putative mechanism responsible for ceramide-induced apoptosis of mammary cancer cells is accumulation of ceramide within the mitochondria. It is now well established that ceramide localization within mitochondria is responsible for mitochondrial dysfunction, including loss of electron potential and cytochrome *c* release, prerequisites for caspase activation (36, 44, 45). The fact that liposomally delivered exogenous C_6 accumulates within caveolin-1-enriched lipid rafts and mitochondria suggests that these two observations may be linked. It has been proposed that ceramide may use caveolae-dependent trafficking as an intracellular delivery route for mitochondrial accumulation (34, 35, 46). In fact, Li et al. have identified an intracellular depot for caveolin-1 in isolated mitochondria, suggesting the existence of a novel pathway of intracellular molecular trafficking, which may be used for delivering specific lipids to multiple cellular compartments (46). Interestingly, caveolin-1 has also been shown to be up-regulated in multidrug-resistant cancer cells (47) and has been suggested to be involved in an intracellular drug trafficking mechanism to shuttle exogenous agent to the plasma membrane where they may be exported by drug efflux pumps. It is possible that caveolin-mediated endocytosis and intracellular trafficking may serve as a pharmacodelivery system for ceramide, allowing for its delivery and accumulation within mitochondria in murine 410.4 mammary adenocarcinoma cells.

Consistent with apoptosis, systemic delivery of liposomal-C_6 induces cytotoxicity of adenocarcinoma solid tumors through decreased cell proliferation (Ki-67 staining) and diminished microvascularization (CD31 staining). Ceramide has been shown to decrease endothelial cell growth and induce apoptosis *in vitro* (23, 48–50). In addition, elevating endogenous ceramide through radiotherapy induces endothelial cell apoptosis *in vivo* (49, 51, 52). In addition, ceramide signaling is required for fenretinide-induced endothelial cell apoptosis and represents a molecular mechanism for the antiangiogenic effects of fenretinide (53). It is also possible that reduced CD31 staining is due to the immature vascular network of smaller ceramide-treated tumors. Regardless of mechanism, our studies are the first demonstration that exogenous short-chain ceramide can be systemically delivered to solid tumor tissue, resulting in significantly reduced tumor microvessel formation as well as induced apoptosis and diminished cellular proliferation.

In agreement with *in vitro* data where liposomal-C_6 was found to be preferentially cytotoxic to murine 410.4 mammary adenocarcinoma cells and not to normal murine HC11 mammary epithelial cells, we observed minimal toxicities in tumor-bearing mice, suggesting that the bioactive concentrations of ceramide achieved in the tumor tissue are not bioactive in normal tissues. Other studies have also suggested that cancerous tissue may generally be more susceptible to the antiproliferative and proapoptotic effects of ceramide analogues than normal tissue (32, 33). Our liposomal formulation may also have fewer side effects due to their pharmacokinetic properties. Steady-state concentrations of ceramide within solid tumors, due to the dysfunctional lymphatic and capillary drainage, may explain preferential adenocarcinoma and associated microvascular cell death. It can be envisioned that the liposomal-C_6 vesicles are trapped in the underdeveloped vasculature of the tumor while being cleared from other tissue compartments. In fact, a two-compartment model calculates a biological half-life of nearly 11 hours, a value consistent with establishing a steady-state therapeutic/cytotoxic dose within the solid tumor tissue. It is critical to note that although the solid tumor tissue is in the peripheral compartment an effective drug concentration is achieved and maintained for a 48-hour treatment period without overt toxicity in the animal.

We have shown systemic efficacy and a favorable pharmacokinetic profile of C_6-incorporated liposomes in two solid tumor models of breast adenocarcinoma. The clinical potential for the delivery of C_6 with additional therapeutic agents in liposomal vesicles is significant. Studies have shown that ceramide may act synergistically with chemotherapeutic agents, such as paclitaxel (54) and fenretinide (55). Thus, delivery of chemotherapeutic agents in C_6-formulated liposomes may further enhance apoptotic actions. Moreover, targeted immunoliposomes are expected to further benefit from C_6 incorporation by enhancing the tumor targeting index. Pegylated liposomal-C_6 vesicles may be conjugated to antibody moieties that target tumor-specific surface antigens, thus permitting targeted therapy of solid tumor and/or metastatic lesions (56, 57). These efforts will be critical in realizing a role for efficient, targeted, and potentially nontoxic ceramide drug delivery in cancer chemotherapy.

Acknowledgments

We thank Nate Sheaffer for assistance with flow cytometry, Young Shin Kim and Dr. Tao Lowe for assistance with the dynamic light scattering particle size. Dr. Amy Fulton for kindly providing the murine 410.4 mammary adenocarcinoma cells, and Dr. Bernd Groner for kindly providing the murine HC11 mammary epithelial cells.

[1] S. Naides, P. Pomianowski, M. Keter, unpublished data.

References

1. Hannun YA. The sphingomyelin cycle and the second messenger function of ceramide. J Biol Chem 1994;269:3125–8.
2. Kolesnick RN, Kronke M. Regulation of ceramide production and apoptosis. Annu Rev Physiol 1998;60:643–65.
3. Spiegel S, Merrill AH Jr. Sphingolipid metabolism and cell growth regulation. FASEB J 1996;10:1388–97.
4. Merrill AH Jr, Schmelz EM, Dillehay DL, et al. Sphingolipids-the enigmatic lipid class: biochemistry, physiology, and pathophysiology. Toxicol Appl Pharmacol 1997;142:208–25.
5. Bose R, Verheij M, Haimovitz-Friedman A, Scotto K, Fuks Z, Kolesnick R. Ceramide synthase mediates daunorubicin-induced apoptosis: an alternative mechanism for generating death signals. Cell 1995;82:405–14.
6. Lucci A, Han TY, Liu YY, Giuliano AE, Cabot MC. Multidrug resistance modulators and doxorubicin synergize to elevate ceramide levels and elicit apoptosis in drug-resistant cancer cells. Cancer 1999;86:300–11.
7. Strum JC, Small GW, Pauig SB, Daniel LW. 1-β-D-Arabinofuranosylcytosine stimulates ceramide and diglyceride formation in HL-60 cells. J Biol Chem 1994;269:15493–7.
8. Haimovitz-Friedman A, Kan CC, Ehleiter D, et al. Ionizing radiation acts on cellular membranes to generate ceramide and initiate apoptosis. J Exp Med 1994;180:525–35.

9. Bruno AP, Laurent G, Averbeck D, et al. Lack of ceramide generation in TF-1 human myeloid leukemic cells resistant to ionizing radiation. Cell Death Differ 1998;5:172–82.
10. Ito A, Horigome K. Ceramide prevents neuronal programmed cell death induced by nerve growth factor deprivation. J Neurochem 1995;65:463–6.
11. Dbaibo GS, Obeid LM, Hannun YA. Tumor necrosis factor-α (TNF-α) signal transduction through ceramide. Dissociation of growth inhibitory effects of TNF-α from activation of nuclear factor-κB. J Biol Chem 1993;268:17762–6.
12. Ballou LR, Chao CP, Holness MA, Barker SC, Raghow R. Interleukin-1-mediated PGE2 production and sphingomyelin metabolism. Evidence for the regulation of cyclooxygenase gene expression by sphingosine and ceramide. J Biol Chem 1992;267:20044–50.
13. Tepper CG, Jayadev S, Liu B, et al. Role for ceramide as an endogenous mediator of Fas-induced cytotoxicity. Proc Natl Acad Sci U S A 1995;92:8443–7.
14. Chang Y, Abe A, Shayman JA. Ceramide formation during heat shock: a potential mediator of α B-crystallin transcription. Proc Natl Acad Sci U S A 1995;92:12275–9.
15. Basu S, Kolesnick R. Stress signals for apoptosis: ceramide and c-Jun kinase. Oncogene 1998;17:3277–85.
16. Hannun YA. Functions of ceramide in coordinating cellular responses to stress. Science 1996;274:1855–9.
17. Bourbon NA, Sandirasegarane L, Kester M. Ceramide-induced inhibition of Akt is mediated through protein kinase Cζ: implications for growth arrest. J Biol Chem 2002;277:3286–92.
18. Jarvis WD, Kolesnick RN, Fornari FA, Traylor RS, Gewirtz DA, Grant S. Induction of apoptotic DNA damage and cell death by activation of the sphingomyelin pathway. Proc Natl Acad Sci U S A 1994;91:73–7.
19. Tepper AD, de Vries E, van Blitterswijk WJ, Borst J. Ordering of ceramide formation, caspase activation, and mitochondrial changes during CD95- and DNA damage-induced apoptosis. J Clin Invest 1999;103:971–8.
20. El Bawab S, Roddy P, Qian T, Bielawska A, Lemasters JJ, Hannun YA. Molecular cloning and characterization of a human mitochondrial ceramidase. J Biol Chem 2000;275:21508–13.
21. Stover T, Kester M. Liposomal delivery enhances short-chain ceramide-induced apoptosis of breast cancer cells. J Pharmacol Exp Ther 2003;307:468–75.
22. Radin NS. Killing tumours by ceramide-induced apoptosis: a critique of available drugs. Biochem J 2003;371:243–56.
23. Mimeault M. New advances on structural and biological functions of ceramide in apoptotic/necrotic cell death and cancer. FEBS Lett 2002;530:9–16.
24. Radin NS. Killing cancer cells by poly-drug elevation of ceramide levels: a hypothesis whose time has come? Eur J Biochem 2001;268:193–204.
25. Shabbits JA, Mayer LD. Intracellular delivery of ceramide lipids via liposomes enhances apoptosis *in vitro*. Biochim Biophys Acta 2003;1612:98–106.
26. Shabbits JA, Mayer LD. High ceramide content liposomes with *in vivo* antitumor activity. Anticancer Res 2003;23:3663–9.
27. Mahoney KH, Fulton AM, Heppner GH. Tumor-associated macrophages of mouse mammary tumors. II. Differential distribution of macrophages from metastatic and nonmetastatic tumors. J Immunol 1983;131:2079–85.
28. Song KS, Li S, Okamoto T, Quilliam LA, Sargiacomo M, Lisanti MP. Co-purification and direct interaction of Ras with caveolin, an integral membrane protein of caveolae microdomains. Detergent-free purification of caveolae microdomains. J Biol Chem 1996;271:9690–7.
29. Rutter CM, Elashoff RM. Analysis of longitudinal data: random coefficient regression modelling. Stat Med 1994;13:1211–31.
30. McEarchern J, Kobie JJ, Mack V, et al. Invasion and metastasis of a mammary tumor involves TGF-β signaling. Int J Cancer 2001;91:76–82.
31. Sweeney EA, Sakakura C, Shirahama T, et al. Sphingosine and its methylated derivative *N*,*N*-dimethylsphingosine (DMS) induce apoptosis in a variety of human cancer cell lines. Int J Cancer 1996;66:358–66.
32. Crawford KW, Bittman R, Chun J, Byun HS, Bowen WD. Novel ceramide analogues display selective cytotoxicity in drug-resistant breast tumor cell lines compared to normal breast epithelial cells. Cell Mol Biol (Noisy-le-grand) 2003;49:1017–23.
33. Struckhoff AP, Bittman R, Burow ME, et al. Novel ceramide analogs as potential chemotherapeutic agents in breast cancer. J Pharmacol Exp Ther 2004;309:523–32.
34. Schroeder F, Gallegos AM, Atshaves BP, et al. Recent advances in membrane microdomains: rafts, caveolae, and intracellular cholesterol trafficking. Exp Biol Med (Maywood) 2001;226:873–90.
35. Carver LA, Schnitzer JE. Caveolae: mining little caves for new cancer targets. Nat Rev Cancer 2003;3:571–81.
36. Birbes H, Bawab SE, Obeid LM, Hannun YA. Mitochondria and ceramide: intertwined roles in regulation of apoptosis. Adv Enzyme Regul 2002;42:113–29.
37. Kester M, Kolesnick R. Sphingolipids as therapeutics. Pharmacol Res 2003;47:365–71.
38. Webb MS, Saxon D, Wong FM, et al. Comparison of different hydrophobic anchors conjugated to poly(ethylene glycol): effects on the pharmacokinetics of liposomal vincristine. Biochim Biophys Acta 1998;1372:272–82.
39. Kolesnick RN, Goni FM, Alonso A. Compartmentalization of ceramide signaling: physical foundations and biological effects. J Cell Physiol 2000;184:285–300.
40. Prinetti A, Chigorno V, Prioni S, et al. Changes in the lipid turnover, composition, and organization, as sphingolipid-enriched membrane domains, in rat cerebellar granule cells developing *in vitro*. J Biol Chem 2001;276:21136–45.
41. Kolesnick R. The therapeutic potential of modulating the ceramide/sphingomyelin pathway. J Clin Invest 2002;110:3–8.
42. Powell DJ, Hajduch E, Kular G, Hundal HS. Ceramide disables 3-phosphoinositide binding to the pleckstrin homology domain of protein kinase B (PKB)/Akt by a PKCζ-dependent mechanism. Mol Cell Biol 2003;23:7794–808.
43. Zhou H, Summers SA, Birnbaum MJ, Pittman RN. Inhibition of Akt kinase by cell-permeable ceramide and its implications for ceramide-induced apoptosis. J Biol Chem 1998;273:16568–75.
44. Di Paola M, Cocco T, Lorusso M. Ceramide interaction with the respiratory chain of heart mitochondria. Biochemistry 2000;39:6660–8.
45. Hearps AC, Burrows J, Connor CE, Woods GM, Lowenthal RM, Ragg SJ. Mitochondrial cytochrome *c* release precedes transmembrane depolarisation and caspase-3 activation during ceramide-induced apoptosis of Jurkat T cells. Apoptosis 2002;7:387–94.
46. Li WP, Liu P, Pilcher BK, Anderson RG. Cell-specific targeting of caveolin-1 to caveolae, secretory vesicles, cytoplasm or mitochondria. J Cell Sci 2001;114:1397–408.
47. Lavie Y, Fiucci G, Liscovitch M. Upregulation of caveolin in multidrug resistant cancer cells: functional implications. Adv Drug Deliv Rev 2001;49:317–23.
48. Lin X, Fuks Z, Kolesnick R. Ceramide mediates radiation-induced death of endothelium. Crit Care Med 2000;28:N87–93.
49. Kolesnick R, Fuks Z. Radiation and ceramide-induced apoptosis. Oncogene 2003;22:5897–906.
50. Matsunaga T, Kotamraju S, Kalivendi SV, Dhanasekaran A, Joseph J, Kalyanaraman B. Ceramide-induced intracellular oxidant formation, iron signaling, and apoptosis in endothelial cells: protective role of endogenous nitric oxide. J Biol Chem 2004;279:28614–24.
51. Alphonse G, Bionda C, Aloy MT, Ardail D, Rousson R, Rodriguez-Lafrasse C. Overcoming resistance to γ-rays in squamous carcinoma cells by poly-drug elevation of ceramide levels. Oncogene 2004;23:2703–15.
52. Pena LA, Fuks Z, Kolesnick RN. Radiation-induced apoptosis of endothelial cells in the murine central nervous system: protection by fibroblast growth factor and sphingomyelinase deficiency. Cancer Res 2000;60:321–7.
53. Erdreich-Epstein A, Tran LB, Bowman NN, et al. Ceramide signaling in fenretinide-induced endothelial cell apoptosis. J Biol Chem 2002;277:49531–7.
54. Mehta S, Blackinton D, Omar I, et al. Combined cytotoxic action of paclitaxel and ceramide against the human Tu138 head and neck squamous carcinoma cell line. Cancer Chemother Pharmacol 2000;46:85–92.
55. Maurer BJ, Melton L, Billups C, Cabot MC, Reynolds CP. Synergistic cytotoxicity in solid tumor cell lines between *N*-(4-hydroxyphenyl)-retinamide and modulators of ceramide metabolism. J Natl Cancer Inst 2000;92:1897–909.
56. Siwak DR, Tari AM, Lopez-Berestein G. The potential of drug-carrying immunoliposomes as anticancer agents. Clin Cancer Res 2002;8:955–6. Commentary of: Park JW, et al. Anti-HER2 immunoliposomes: enhanced efficacy due to targeted delivery. Clin Cancer Res 2002;8:1172–81.
57. Nam SM, Kim HS, Ahn WS, Park YS. Sterically stabilized anti-G(M3), anti-Le(x) immunoliposomes: targeting to B16BL6, HRT-18 cancer cells. Oncol Res 1999;11:9–16.